AIAA JOURNAL
Vol. 34, No. 2, February 1996

Effects of Asymmetric Inflow on Near-Field Propeller Noise

Johan B. H. M. Schulten*
National Aerospace Laboratory NLR, 8300 AD Emmeloord, The Netherlands

The aerodynamic and subsequent acoustic effects of nonaxial inflow on wide-chord, advanced high-speed propellers are studied by means of a lifting surface theory. Starting from the flow equations for a perturbed, axially subsonic flow, expressions are derived for the pressure and velocity field of a propeller. By using a representation of Green's function in separated, cylindrical coordinates the boundary condition at the hub is naturally incorporated. Application of the boundary condition at the blade surfaces yields an integral equation for the unknown pressure jump distribution over the blades that is solved numerically. The method is applied to study the near-field acoustic effects of propellers in uniform upwash and downwash at low and high speeds. Typical examples show that, for moderate speed, substantial reductions of the side line peak level of the order of 5 dB are possible for the proper amount of downwash. At high speed, however (flight Mach number 0.75, helical tip speed supersonic), downwash does not yield any significant sound reduction.

Nomenclature

B = number of blades
c_∞ = ambient speed of sound
$D(r)$ = angular position of zeroth blade at $t = 0$, $x = 0$, [Eq. (16)]
$\boldsymbol{F}$ = force field [Eq. (5)]
G = Green's function [Eq. (11)]
$\boldsymbol{g}_c(r)$ = blade camber vector [Eq. (18)]
$\boldsymbol{g}_t(r)$ = blade thickness vector [Eq. (18)]
$\boldsymbol{g}_0(r)$ = vector normal to blade helical surface [Eq. (18)]
$H_m^{(2)}$ = second kind Hankel function of order m
h = hub/tip ratio
$\boldsymbol{i}_x, \boldsymbol{i}_r, \boldsymbol{i}_\theta$ = unit vectors in x, r, θ directions (Fig. 1)
J_m = Bessel function of the first kind of order m
k = circumferential periodicity of incident velocity
M = axial flow Mach number (Fig. 1)
p = pressure induced by blade row
Q = displacement source strength [Eq. (4)]
R_n = reduced Green's function [Eq. (14)]
r = radial coordinate
S = blade surface function [Eq. (15)]
t = time coordinate
$\boldsymbol{v}$ = velocity induced by blade row
$\boldsymbol{W}_k$ = kth Fourier component of incident field [Eq. (22)]
$\boldsymbol{w}$ = velocity of incident field
x = axial coordinate
α = axial wave number [Eq. (9)]
$\beta(r)$ = blade angle distribution (Fig. 3)
$\gamma(\alpha, \omega)$ = radial wave number [Eq. (12)]
ΔC_p = Δp scaled on $\rho_\infty c_\infty^2 (M^2 + \Omega^2 r^2)/2$
Δp = blade pressure jump distribution $(p^+ - p^-)$
$\Delta\phi(x, r)$ = angular blade thickness (Fig. 3)
δ = upwash angle, tilt angle
ε = small perturbation parameter
θ = circumferential coordinate (Fig. 1)
ξ = axial source coordinate (Fig. 1)
$\boldsymbol{\xi}$ = source position vector
ρ = radial source coordinate, air density
τ = source time
ϕ = circumferential source coordinate (Fig. 1)
Ω = tangential tip Mach number (Fig. 1)
ω = Helmholtz number (nondimensional frequency) [Eq. (9)]
ω_m = $\omega - m\Omega$
$\langle\cdot\rangle$ = inner product of two three-dimensional vectors

Subscripts

F = force related
H = helical
L = leading edge
Q = displacement related
T = trailing edge
∞ = ambient, at infinity

Superscripts

(a) = anechoic
$+$ = blade lower side
$-$ = blade upper side
$\tilde{}$ = in time domain
$\hat{}$ = axially Fourier transformed

Received April 12, 1995; presented as Paper 95-164 at the CEAS/AIAA First Joint Aeroacoustics Conference, Munich, Germany, June 12–15, 1995; revision received Oct. 3, 1995; accepted for publication Oct. 10, 1995.

*Senior Research Engineer, Aeroacoustics Department, P.O. Box 153. Senior Member AIAA.

Introduction

WHEREAS the interior noise level of jet aircraft can compete with luxury cars, propeller driven aircraft generally suffer from an unpleasantly loud cabin noise. As opposed to fan noise, which is the major noise component for current jetliners, the absence of a shielding duct permits the pressure distortions generated by the rotating propeller blades to impinge directly on the fuselage. In particular for wing mounted propellers, the distance to the fuselage often is so small that even at moderate flying speeds a very high sound pressure level (typically, 140 dB) is found in the area of minimum tip clearance.

It is well known that the noise on opposite sides of an installed propeller can be quite different. The reason is that the inflow to the propeller is, in general, not perfectly axisymmetric. The propeller axis is not necessarily coincident with the flight direction, and the proximity of wing and fuselage also contribute to an asymmetric inflow. These so-called installation effects lead to a periodically varying air load of the blades and, as a result, to an asymmetric propeller sound field. Since propellers usually rotate in the same direction, this means that the left and right propeller give, in general, an asymmetric contribution to the acoustic excitation of the fuselage.

To be able to compute the sound field of a propeller, the aerodynamic field in the immediate neighborhood of the blades has to be known first. Thus, in practice, there are always two different problems to be solved; the aerodynamic and the acoustic.

Whereas the aerodynamic calculations are made at all possible levels of sophistication, the acoustic calculations are almost invariably based on the Ffowcs Williams and Hawkings[1] (FW–H) version of the acoustic analogy. If the quadrupole source strength in the FW–H formulation is suppressed, the result is identical to the equation for the pressure derived from the linearized aerodynamics of the lifting surface approximation, which will be used in the present study. This approximation is accurate for small distortions, i.e., $\mathcal{O}(\varepsilon)$, of a uniform, high Reynolds number flow. These conditions are sufficiently satisfied for most of the operating conditions of propellers and propfans.

An essential point in linear theories is the construction of Green's function of the problem considered, since there is a considerable freedom of choice in its representation. For free space there are two usual ways to express Green's function, the time-domain and the frequency wave number formulation, each having its own merits and drawbacks. Both describe exactly the same acoustic field of an impulsive point source but have an entirely different appearance. The time-domain formulation perhaps is the most appealing physically because it displays the spherical propagation of an acoustic pulse. It was introduced in propeller acoustics by Gutin[2] in 1936 and extended in 1953 by Garrick and Watkins[3] to include the effects of forward speed. More recently, time-domain methods have been used by Farassat,[4] Long and Watts,[5] and several other researchers. The outstanding advantage of the time-domain formulation is that it can be used for arbitrary bodies in any motion. As a result it can be applied equally well to propellers in axial flow as to tilted propellers with helicopter rotors in forward flight as the extreme case.

In its pure form the time-domain method yields the time signal of the pressure generated by the propeller. Especially at higher helical speeds this signal can be rather peaky, and a large number of time points is required for an accurate description. If the main interest is in a few lower blade passing harmonics only, it is then useful to adopt the Fourier transform in time of the spherical, time-domain Green's function to extract directly a selected harmonic from the total propeller frequency spectrum.[3] Recently, this direct frequency domain representation was used by Hanson[6] to study the sound field of a tilted propeller.

The frequency wave number representation naturally emerges by taking not only the Fourier transform in time but also in cylindrical space coordinates of the governing equation for Green's function. Early compressible propeller formulations based on this representation were derived by Kondo[7] and Davidson,[8] whereas more recently lifting surface methods in this category were developed by Hanson[9] and Schulten.[10,16] An advantage of the frequency wave number approach is that, in contrast to the spherical representation, boundary conditions at coordinate planes can be incorporated in Green's function. As will be shown in the present study, radial boundary conditions at a hub can be imposed that makes the approach applicable to propfans with nonnegligible hubs. Another advantage is that the field of the blade row is given as an expansion of time–space harmonics. This is most convenient and efficient in acoustic applications where the harmonic distribution over a whole surface is to be computed, such as in diffraction around a fuselage. Finally, integrations need to be performed for one single blade only, since the combined effect of all blades can be taken into account analytically.

These benefits are partly offset by the mathematical complexity of the formulation. Further, an important restriction of the frequency wave number approach is that the main flow direction has to coincide with the propeller axis, and hence the asymmetry of the inflow must be small. For a tilted propeller even then additional effects arise in the far-field radiation that can be only accounted for by special techniques such as Hanson's[11] wobbling modes or, alternatively, by an intermediate Kirchhoff surface enclosing the propeller.

Although the problem of a propeller in asymmetric flow has been studied theoretically[11–13] as well as experimentally[13–15] by several authors previously, the picture of how even the most simple form of installation effects, viz., up- and downwash, affect propeller sound is far from complete.

In the present paper a frequency wave number lifting surface formulation[16] is used to solve both the aerodynamic and the acoustic problem for advanced and conventional propellers. The existing linear theories are extended by a full account of the presence of a hub. Also the often neglected effect of blade-thickness-induced velocity on the aerodynamic loading is incorporated. The method is applied to compute the effects of an asymmetric inflow on propeller noise in the near field, where the unsteady loading effect predominates in the radiation. By comparison with existing experimental aerodynamic and acoustic data for a propfan and for a conventional propeller, the validity of the method is demonstrated. In addition, some of the results for a conventional propeller are also compared with those of a lifting line theory. In particular, the possibilities of a beneficial reduction of near-field side line noise by downwash are explored.

Analysis

Governing Equations

We consider a single propfan placed in an inviscid, uniform, subsonic main flow of Mach number M $(0 < M < 1)$. To obtain a nondimensional formulation, the mass density ρ_∞ and speed of sound c_∞ of the main flow and the blade tip radius are taken as scaling parameters. With this scaling the pressure and density perturbations of the main flow become to leading order identical. If the x axis is chosen along the hub axis (Fig. 1) with the positive direction downstream, the governing, i.e., the leading order, flow equations are the linearized Euler equations for the (dimensionless) perturbation pressure $\tilde{p}$ and velocity $\tilde{v}$

$$\frac{\mathrm{D}\tilde{p}}{\mathrm{D}t} + \langle \nabla \cdot \tilde{v} \rangle = 0 \tag{1}$$

and

$$\frac{\mathrm{D}\tilde{v}}{\mathrm{D}t} + \nabla \tilde{p} = \mathbf{0} \tag{2}$$

where the linearized material derivative $\mathrm{D}/\mathrm{D}t = \partial/\partial t + M\partial/\partial x$. A tilde indicates that the variable is understood to be in the time domain; the absence of an overmark implies that the variable is in the frequency domain.

To formulate the boundary condition at the blade surfaces, a (sufficiently smooth) function S is introduced with the property $S > 0$ outside the blades and $S < 0$ inside. Note that $S(\boldsymbol{x}, t) = 0$ not only describes the blades' shape but also their motion. Since the vector ∇S is normal to the blade surface, the boundary condition of flow tangency at the moving blade surfaces can be written as (Fig. 2)

$$\lim_{S \downarrow 0} \langle \nabla S \cdot \tilde{v} \rangle = \langle \nabla S \cdot (\Omega r \boldsymbol{i}_\theta - M \boldsymbol{i}_x - \tilde{w}) \rangle_{S=0} \tag{3}$$

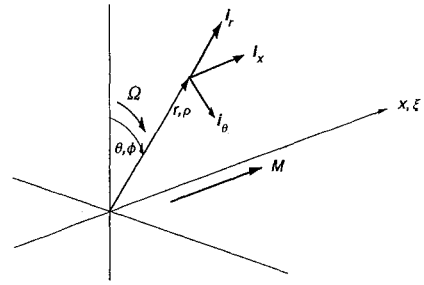

Fig. 1 Coordinate system.

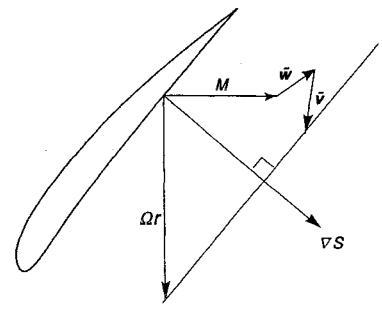

Fig. 2 Boundary condition at blade surface.

where $\tilde{w}$ denotes the incident velocity field, in the present context consisting of a nonuniformity of the main flow, not generated by the blade row considered.

Obviously, the flow equations [Eqs. (1) and (2)] are valid only outside the blades. Following Crighton,[17] however, we can make them formally valid throughout the domain considered by multiplication with the Heaviside function of S : $H(S)$. Next, $H(S)$ is linked to the flow variables by applying the chain rule of differentiation.

The interesting point of this manipulation is that the differential operator automatically creates sources at the blade surfaces, i.e., a term $\tilde{Q}\delta(S)$ in the right-hand side of Eq. (1) and a term $\tilde{F}\delta(S)$ in the right-hand side of Eq. (2), where

$$\tilde{Q} = \tilde{\rho}\frac{\mathrm{D}S}{\mathrm{D}t} + \langle\tilde{v}\cdot\nabla S\rangle \tag{4}$$

and

$$\tilde{F} = \tilde{v}\frac{\mathrm{D}S}{\mathrm{D}t} + \tilde{p}\nabla S \tag{5}$$

Elimination of the velocity $\tilde{v}$ from Eqs. (1) and (2) yields the following convected-wave equation for the pressure

$$\left(\nabla^2 - \frac{\mathrm{D}^2}{\mathrm{D}t^2}\right)\tilde{p} = -\frac{\mathrm{D}}{\mathrm{D}t}[\tilde{Q}\delta(S)] + \langle\nabla\cdot[\tilde{F}\delta(S)]\rangle \tag{6}$$

By means of Green's function $\tilde{G}$ for the convected wave operator [in the left-hand side of Eq. (6)] the complete pressure field can be written in terms of just the conditions at the blade surfaces. In the present problem Green's function can be interpreted as the pressure field of an impulsive point source at the point ξ that "fires" at time τ.

We can now formally solve Eq. (6) by integrating (by parts) over the source distribution in space and time to obtain the thickness noise

$$\tilde{p}_Q = \int\int\int\int -\frac{\mathrm{D}\tilde{G}}{\mathrm{D}\tau}\tilde{Q}(\xi,\tau)\delta(S)\,\mathrm{d}\xi\,\mathrm{d}\tau \tag{7}$$

and the loading noise

$$\tilde{p}_F = \int\int\int\int \langle\nabla_0\tilde{G}\cdot\tilde{F}(\xi,\tau)\rangle\delta(S)\,\mathrm{d}\xi\,\mathrm{d}\tau \tag{8}$$

where $\mathrm{D}/\mathrm{D}\tau = \partial/\partial\tau + M\partial/\partial\xi$ and ∇_0 is the gradient operator with respect to the source coordinates. With the quadrupole term suppressed, these formulas are essentially equivalent to Goldstein's[18] Eq. (4.10). To obtain the blade surface pressure the boundary condition of flow tangency [Eq. (3)] has to be applied. This in turn requires the velocity field induced by the blades. To find the velocity we use the momentum equation with the source term $\tilde{F}$ and separate $\tilde{v}$ into a velocity field originating from $\tilde{Q}$ (via $\tilde{p}_Q$) and one induced by $\tilde{F}$ (via $\tilde{p}_F$ and $\tilde{F}$). When we now take Fourier transforms in time and axial direction, the velocity caused by $\tilde{Q}$ in (α,ω) space is found to be

$$\hat{v}_Q = \frac{-1}{i(\omega+M\alpha)}\left(i\alpha\boldsymbol{i}_x + \boldsymbol{i}_r\frac{\partial}{\partial r} + \boldsymbol{i}_\theta\frac{\partial}{r\partial\theta}\right)\hat{p}_Q \tag{9}$$

Similarly, we find for the velocity caused by $\tilde{F}$

$$\hat{v}_F = \frac{1}{i(\omega+M\alpha)}\left[\hat{F} - \left(i\alpha\boldsymbol{i}_x + \boldsymbol{i}_r\frac{\partial}{\partial r} + \boldsymbol{i}_\theta\frac{\partial}{r\partial\theta}\right)\hat{p}_F\right] \tag{10}$$

where (x, r, θ) is a cylindrical coordinate system (Fig. 1).

Green's Function

In the preceding section we have already assumed the existence of a Green's function $\tilde{G}$ for the convected-wave operator. In this section we will construct $\tilde{G}$ such that it not only satisfies an outward radiation condition but also the boundary condition at a hub. This is made possible by representing $\tilde{G}$ as a superposition of circumferential and axial waves as follows:

$$\tilde{G}(x,r,\theta,t\mid\xi,\rho,\phi,\tau) = \frac{1}{(2\pi)^3}\sum_{n=-\infty}^{\infty}\exp[in(\theta-\phi)]$$
$$\times\int_{-\infty}^{\infty}\int_{-\infty}^{\infty}\exp\{i[\omega(t-\tau)+\alpha(x-\xi)]\}R_n(\alpha,r,\omega\mid\rho)\,\mathrm{d}\alpha\,\mathrm{d}\omega \tag{11}$$

where R_n is the "reduced Green's function." Now we introduce the radial wave number γ that is related to the axial wave number α and the Helmholtz number (dimensionless frequency) ω as

$$\gamma^2 = (\omega+M\alpha)^2 - \alpha^2 \tag{12}$$

If the branch cuts of γ are taken such that $\mathrm{Im}\,\gamma \le 0$ throughout the complex α plane, the anechoic, free space reduced Green's function is given by[16]

$$R_n^{(a)} = -i(\pi/2)\left[J_n(\gamma r)H_n^{(2)}(\gamma\rho)H(\rho-r)\right.$$
$$\left.+J_n(\gamma\rho)H_n^{(2)}(\gamma r)H(r-\rho)\right] \tag{13}$$

which is basically equivalent to the expressions used by Kondo[7] and Hanson.[9] Propfans, however, usually have a relatively large hub, which can hardly be ignored. It can be expected that the presence of a hub manifests itself as a distribution of cylindrical waves $A(\alpha)H_n^{(2)}(\gamma r)$ emanating from the hub surface, similar to the diffraction of sound by an aircraft fuselage. From the radial component of the momentum equation (2) it follows that the boundary condition at a hard-walled hub is given by $\partial R_n/\partial r = 0$. This condition determines the amplitude A such that

$$R_n = R_n^{(a)} + i(\pi/2)\left[J_n'(\gamma h)/H_n^{(2)'}(\gamma h)\right]H_n^{(2)}(\gamma\rho)H_n^{(2)}(\gamma r) \tag{14}$$

It is to be noted that this modeling implies an infinitely long hub cylinder, which, of course, is only a first approximation of reality.

Blade Geometry

To describe the rotating blade surfaces by $S = 0$, it is convenient to introduce separate functions for upper (−) and lower (+) surfaces. The angular coordinate of the leading edge of the zeroth blade at $t = 0$ is given by $\phi_L(r)$, whereas $x_L(r)$ denotes its axial coordinate (Fig. 3). If the number of blades is denoted by B, the surface of the jth blade is given by

$$S_j^{\pm} = \pm\{\theta - [D - (\Omega/M)x + \Omega t + j(2\pi/B)$$
$$+\phi_c \pm (\Delta\phi/2)]\} = 0 \tag{15}$$

where

$$D(r) = \phi_L(r) + (\Omega/M)x_L(r) \tag{16}$$

is the angular position of the helical surface associated with the zeroth blade at $t = 0, x = 0$. Here, ϕ_c describes the mean camber line of the blade section at radius r relative to the undisturbed helical

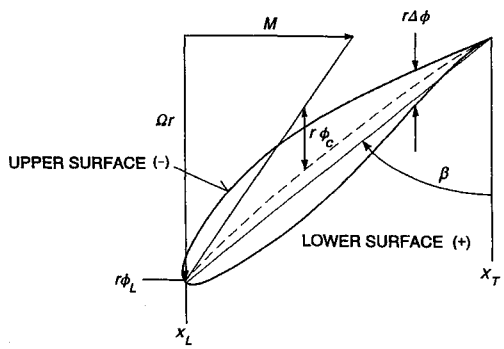

Fig. 3 Blade intersection with cylindrical surface (r = const); for clarity $\Delta\phi$ and ϕ_c have been exaggerated with respect to realistic situations.

line, whereas $\Delta\phi$ describes the blade thickness in the angular coordinate. Note that ϕ_c also includes the angle of attack of the blade section. Both ϕ_c and $\Delta\phi$ are of $\mathcal{O}(\varepsilon)$ and it is easily shown that DS/Dt on the moving blade surface is also of $\mathcal{O}(\varepsilon)$. This implies that the terms in $\tilde{Q}$ and $\tilde{F}$ containing DS/Dt are of $\mathcal{O}(\varepsilon^2)$ and can be neglected in the present linear modeling.

The normal vector ∇S can now be written as

$$\nabla S^{\pm} = \pm\{\boldsymbol{g}_0(r) - \boldsymbol{g}_c(x,r)\} - \tfrac{1}{2}\boldsymbol{g}_t(x,r) \tag{17}$$

where

$$\boldsymbol{g}_0(r) = \begin{bmatrix} \Omega \\ \overline{M} \\ -D'(r) \\ \dfrac{1}{r} \end{bmatrix}, \qquad \boldsymbol{g}_c(x,r) = \begin{bmatrix} \dfrac{\partial\phi_c}{\partial x} \\ \dfrac{\partial\phi_c}{\partial r} \\ 0 \end{bmatrix}$$

$$\boldsymbol{g}_t(x,r) = \begin{bmatrix} \dfrac{\partial\Delta\phi}{\partial x} \\ \dfrac{\partial\Delta\phi}{\partial r} \\ 0 \end{bmatrix} \tag{18}$$

from which it is obvious that, for blades without lean, $D(r)$ is constant since then the radial component of $\boldsymbol{g}_0$ vanishes. To avoid bending stresses by centrifugal loads propeller blades have zero or negligible lean.

Blade Displacement Pressure Field

Using the boundary condition at the blade surfaces [Eq. (3)] we find for the displacement source strength

$$\tilde{Q}^{\pm} = \pm\left[M\frac{\partial\phi_c}{\partial\xi} - \langle\tilde{\boldsymbol{w}}^{\pm}\cdot\boldsymbol{g}_0(\rho)\rangle\right] + \frac{M}{2}\frac{\partial\Delta\phi}{\partial\xi} \tag{19}$$

which contains known quantities only. When we substitute this expression in Eq. (7) and integrate over the source coordinates (ξ, ρ, ϕ, τ), it appears that the integrals with respect to ϕ and τ can be evaluated analytically. The integral in ϕ can be evaluated exactly via the delta function of S, whereas the integral in τ simply is the Fourier transform of an exponential that yields $2\pi\delta(\omega + n\Omega)$. Ignoring geometrically induced terms of higher order, we obtain an expression in which the integration over upper and lower surfaces has been combined into a single chordwise integral from leading edge (x_L) to trailing edge (x_T).

Now summation over the blades ($j = 0, B-1$) can be carried out analytically by using the sum of the geometric progression to B terms, or equivalently by using symmetry arguments. The summation yields a factor B if n equals a multiple of the number of blades B and zero otherwise. Thus, the interference of the blades is taken into account analytically, and we have to consider only one blade in the calculations. Compared to the time-domain method this is an important advantage of the present formulation in separated, cylindrical coordinates. Transforming back to the physical domain as in Eq. (11) for $\tilde{G}$, we obtain for the thickness noise

$$\tilde{p}_Q = \frac{iBM}{(2\pi)^2}\sum_{n=-\infty}^{\infty}\exp[im(\theta-\Omega t)]\int_{-\infty}^{\infty}(M\alpha - m\Omega)\exp(i\alpha x)$$
$$\times\int_h^1 R_m(\alpha, r, -m\Omega\mid\rho)\exp[-imD(\rho)]$$
$$\times\int_{x_L(\rho)}^{x_T(\rho)}\exp\left[i\left(\frac{m\Omega}{M}-\alpha\right)\xi\right]\rho\frac{\partial\Delta\phi}{\partial\xi}\,d\xi\,d\rho\,d\alpha \tag{20}$$

where the circumferential wave number $m = -nB$. This expression clearly displays the time–space $(\theta - \Omega t)$ dependence one expects for a rotating blade row. Note that this expression also includes the steady ($n = 0$) effect of blade thickness displacement. Note also that Eq. (20) is exactly the same expression as we would have obtained by prescribing a source strength $M\rho\partial\Delta\phi/\partial\xi$ at the undisturbed helical surfaces to which the blades reduce for $\Delta\phi, \phi_c \to 0$.

Blade Loading Pressure Field

Using the definition of $\tilde{F}$ [Eq. (5)], we find that in the present case $\tilde{\boldsymbol{F}}_j^{\pm} = \pm\tilde{p}_j^{\pm}\boldsymbol{g}_0(\rho)$ to leading order. The surface pressure at the jth blade $\tilde{p}_j$ is, in general, an unknown quantity at this stage. Since all blades are assumed to be identical and equally spaced, the aerodynamic conditions resulting from the blade geometry must also be identical from blade to blade. To allow a summation over the blades, we expand the incident field $\tilde{w}$ into a circumferential Fourier series.

Since the problem is linear we may consider the response of the blade row to the kth Fourier component and find the complete solution later by summation over k. Then, the conditions at the surface of blade j differ only by a factor $\exp[ikj2\pi/B]$ from the conditions at blade 0. We now obtain after integration over the source domain an expression in which the force distributions Δp are effectively located at the undisturbed helical surfaces. After the summation over the blades has again been carried out analytically, the inverse transform to the physical domain yields the loading pressure field

$$\tilde{p}_F = \frac{-iB}{(2\pi)^3}\sum_{n=-\infty}^{\infty}\int_{-\infty}^{\infty}\exp(i\omega_m t)\exp(im\theta)\int_{-\infty}^{\infty}\exp(i\alpha x)$$
$$\times\int_h^1\rho\exp[-imD(\rho)]\left\langle\boldsymbol{g}_0(\rho)\cdot\begin{bmatrix}\alpha\\ \dfrac{i\partial}{\partial\rho}\\ \dfrac{m}{\rho}\end{bmatrix}\right\rangle$$
$$\times R_m(\alpha, r, \omega_m\mid\rho)\int_{x_L(\rho)}^{x_T(\rho)}\exp\left[i\left(\frac{m\Omega}{M}-\alpha\right)\xi\right]$$
$$\times\Delta p(\xi,\rho,\omega)\,d\xi\,d\rho\,d\omega \tag{21}$$

where $\omega_m = \omega - m\Omega$ and $m = k - nB$.

Expression (21) is called the solution to the direct or acoustic problem. It can be computed as soon as Δp is known. The determination of Δp, which is sometimes called the deductive or aerodynamic problem, will be briefly addressed in the next section. In general, Δp has a pure tone spectrum and then the ω integral is trivial. Further, in most acoustic problems $r > 1$ and then the Hankel function $H_n^{(2)}(\gamma r)$ can be taken out of the reduced Green's function under the integral in ρ. This means that the (ξ, ρ) integral over the blade surface then only depends on n and α. In other words, for the harmonic pressure at another x, r position only the outer α integral has to be recomputed. By appropriate programming the pressure data along a side line are computed in parallel. Additional side lines can be computed in much less computer time than the first one.

Pressure Jump Distribution

Using the actual source distribution and force field it is now relatively straightforward to deduce the displacement velocity field $\tilde{v}_Q$ and the loading velocity field $\tilde{v}_F$ of a complete propeller. The only unknown quantity in these lengthy expressions[16,19] is the pressure jump distribution Δp over the zeroth blade. To solve Δp we have to apply the boundary condition Eq. (3) at the blade surfaces. Combining the boundary conditions at upper and lower blade surfaces as in Ref. 16, we obtain the following integral equation for the pressure jump distribution Δp:

$$[\langle\boldsymbol{g}_0\cdot\tilde{\boldsymbol{v}}_F\rangle]_{\theta=D+\Omega(t-x/M)}$$
$$= \left[M\frac{\partial\phi_c}{\partial x} - \langle\boldsymbol{g}_0\cdot\tilde{\boldsymbol{v}}_Q\rangle - \langle\boldsymbol{g}_0\cdot\tilde{\boldsymbol{W}}_k e^{ik\theta}\rangle\right]_{\theta=D+\Omega(t-x/M)} \tag{22}$$

Note the presence of the kth Fourier component $\tilde{\boldsymbol{W}}_k(x, r, t)$ of the incident velocity field in the right-hand side of Eq. (22). For a uniform upwash achieved by placing the propeller axis at an angle of attack δ the circumferential Fourier coefficients all are zero except for $k = \pm 1$, when $\boldsymbol{W}_{\pm 1} = (M/2)\tan\delta[\boldsymbol{i}_r \pm i\boldsymbol{i}_\theta]$. It is obvious that the contribution of the $k = -1$ term is complex conjugate to the $k = 1$ term.

Also note the presence of the blade displacement velocity $\tilde{v}_Q$ in the right-hand side of Eq. (22). This term achieves the coupling between

thickness and steady loading that occurs in multiple body aerodynamics and in isolated, nonplanar lifting surface configurations. Since a propeller is both multibladed and twisted, this interference, for propellers first indicated by Van de Vooren and Zandbergen,[20] is in general present.

As discussed in detail in Refs. 16 and 19, this pressure jump distribution is expanded into a series of suitably chosen basis functions. After application of a Galerkin projection the integral equation transforms into a set of linear equations that is solved numerically. In general, this process takes considerably more computer time (typically 8 h on a 486/50 personal computer) than a simple acoustic calculation, which usually takes not more than a mere 30 s/harmonic for a complete side line of 64 points.

For the numerical results in this study the control parameters of the accuracy of the complete computation process were set such that the plots of the results were fully converged to their final shape. In other words, a higher numerical accuracy would not be visible on a standard diagram, whether linearly or logarithmically (decibel) scaled.

Numerical Results for Propfans

Aerodynamic Validation

The validation of the method with regard to the steady aerodynamics is reported in Ref. 19. For the validation of the unsteady aerodynamics the NASA 8-bladed SR7a propfan was chosen. Apart from extensive experimental data for uniform flow, unsteady blade pressures measured[13] in the S1 wind tunnel in France for a uniform upwash are also available for this propeller in a 2-blade version. In Figs. 4 and 5 a comparison is made between the present theory, calculations based on the full Euler equations,[13] and measurements of the pressure jump distribution at a relative radius of 0.641. It appears that the results of the lifting surface theory and the Euler calculations are in close agreement. The discrepancy with the experimental data in the forward part of the chord most probably results from the presence of a leading-edge vortex, a phenomenon not modeled in both (inviscid) theories. The comparison is limited to the first harmonic since the higher harmonics are negligibly small.

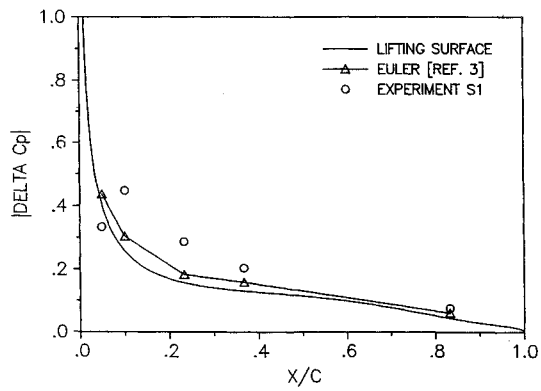

Fig. 4 Absolute value of unsteady pressure jump SR7a propeller, two-bladed version, $M = 0.5$, $J = 3.062$, 3-deg upwash, first harmonic, and $r = 0.641$.

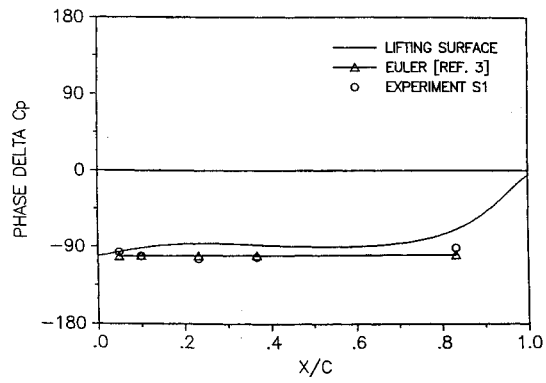

Fig. 5 Phase of unsteady pressure jump SR7a propeller; conditions as in Fig. 4.

SR7a at Mach = 0.6 Forward Speed

As a first example for the acoustic calculations a case of moderate forward speed (Mach number $M = 0.6$) was selected. The advance ratio J for this case is 3.3 and the blade angle (at $r = 0.75$) 60.2 deg. Aerodynamically this is a moderately loaded case ($C_T = 0.37$, $C_P = 1.58$). All sound pressure level (SPL) calculations in the present paper refer to standard atmospheric conditions at sea level.

The acoustic pressure level along a side line (90 deg) at a relative radius of 1.5 at 4 upwash angles is presented in Fig. 6. This uniform upwash is equivalent to an angle of attack of the propeller axis. It is clear that the pressure level rises monotonically with upwash angle at an initial rate of about 1.2 dB/deg in the peak region. Note that in the forward arc the increase is only half of that in the aft arc.

Figure 7 presents the results of an increasing downwash along the same side line. Here the picture is somewhat different. After an initial decrease (−2.5 deg) the peak sound level starts to rise again somewhere between −2.5 and −5 deg. At −7.5 deg the peak level is almost back at the level of 0 deg. At the same time it is noted that the position of the peak moves downstream. It seems that the possibilities for reduction of the noise by downwash for this case are limited to some 4 dB. There are at least two reasons for such a limitation. First, the downwash only affects the loading part of the noise and leaves the thickness part unaltered. Second, the acoustic effect of a reduced loading at the observation side is partly compensated by the increased loading at the opposite side of the propeller.

To get a more comprehensive picture of the acoustic near field of this case, the real and imaginary parts of the first harmonic, nondimensional pressure are plotted over the area $x = (-2, 2)$, $r = (1.2, 3)$. Figures 8 and 9 present the results for an upwash of 3 deg and Figs. 10 and 11 for a downwash of 3 deg. The reduction of peak amplitudes in this linear plot is spectacular. At the same time a negative peak just downstream of the upwash peak appears in Figs. 10 and 11. This peak grows rapidly as the downwash is further increased and thus limits the total possible reduction. Another observation that can be made is the considerable acoustic benefit of a larger tip clearance, especially in the upwash case.

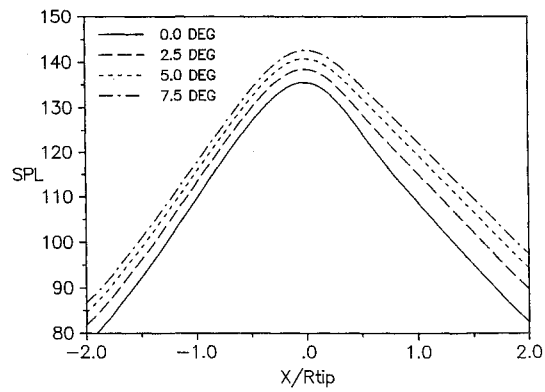

Fig. 6 SR7a propfan in uniform upwash, first harmonic, $M = 0.6$, $J = 3.3$, blade angle 60.2 deg, $r = 1.5$, and $\theta = 90$ deg.

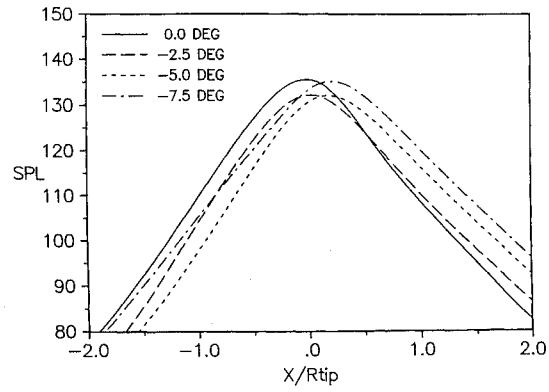

Fig. 7 SR7a propfan in uniform downwash, first harmonic; conditions as in Fig. 6.

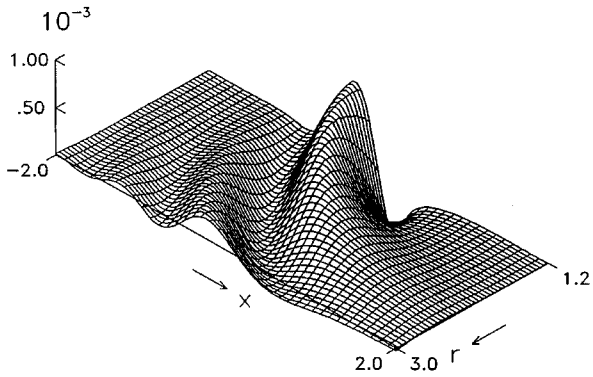

Fig. 8 Real part of first harmonic pressure field of SR7a propfan at 3 deg of upwash; conditions as in Fig. 6.

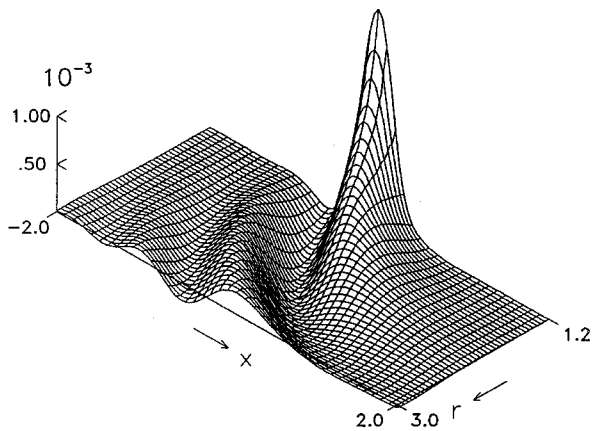

Fig. 9 Imaginary part of first harmonic pressure field of SR7a propfan at 3 deg of upwash; conditions as in Fig. 6.

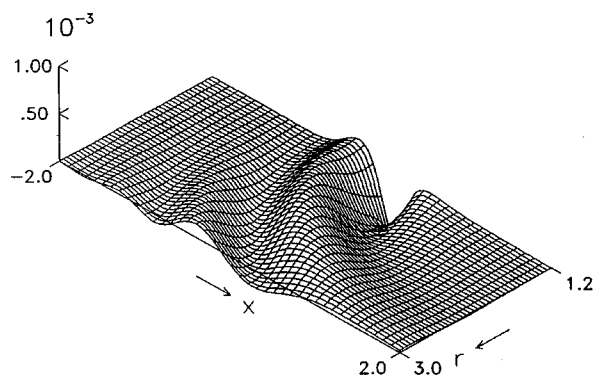

Fig. 10 Real part of first harmonic pressure of SR7a propfan at 3 deg of downwash; conditions as in Fig. 6.

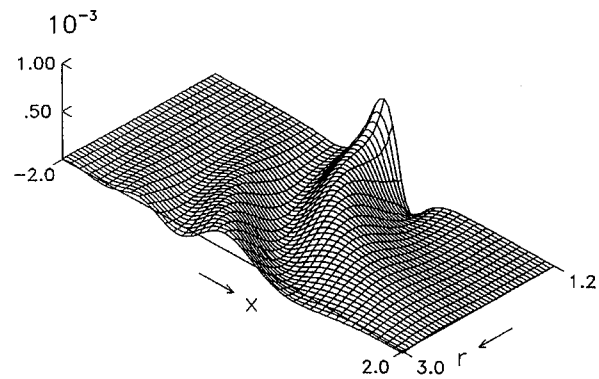

Fig. 11 Imaginary part of first harmonic pressure of SR7a propfan at 3 deg of downwash; conditions as in Fig. 6.

SR7a at Mach = 0.75 Forward Speed

Advanced propellers are designed to operate at high subsonic cruise speeds. Therefore, it is interesting to investigate their acoustic behavior at cruise conditions. In Fig. 12 the SPL of the SR7a at a forward Mach number of 0.75 is given for various upwash angles. The helical tip Mach number for this case is just sonic. The calculated aerodynamic loading is moderate ($C_T = 0.31$, $C_P = 1.34$). First note the overall SPL increase of about 20 dB compared to the previous case. The effect of upwash on the peak SPL is rather modest: only 0.6 dB per degree of upwash. Similarly, in Fig. 13 only 3-dB reduction is attained at a downwash of 5 deg.

In Figs. 14 and 15 the results for a highly loaded case ($C_T = 0.48$, $C_P = 2.07$) with supersonic helical tip speed ($M_H = 1.07$) are presented. With only 0.4 dB per degree we observe here an even lower effect of upwash and downwash. It is concluded that for this case the possibilities for sound reduction by downwash are only marginal. Most probably this is a consequence of source noncompactness, which becomes significant at high speeds. It means that

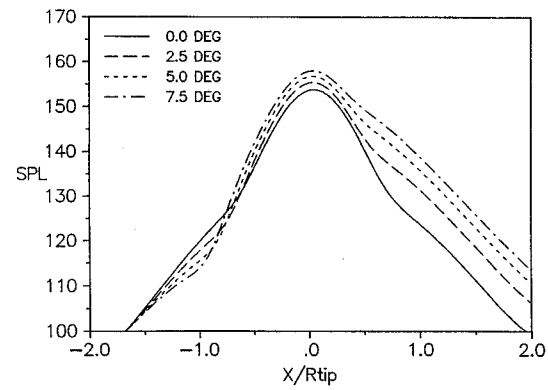

Fig. 12 SR7a propfan in uniform upwash, first harmonic, $M = 0.75$, $J = 3.57$, blade angle 60.2 deg, $r = 1.5$, and $\theta = 90$ deg.

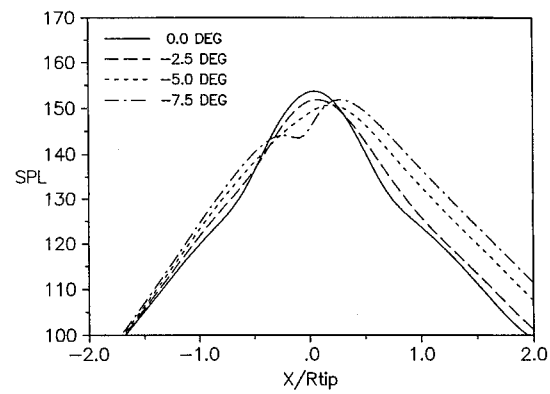

Fig. 13 SR7a propfan in uniform downwash, first harmonic; conditions as in Fig. 12.

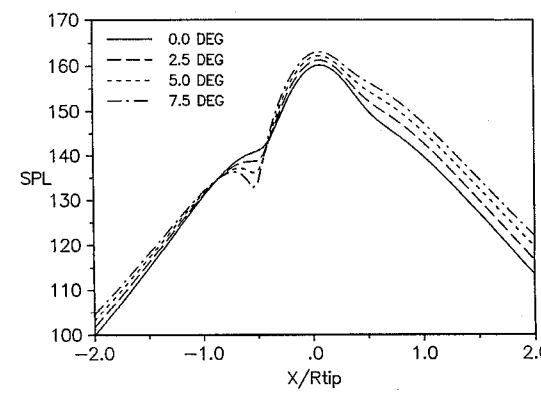

Fig. 14 SR7a propfan in uniform upwash, first harmonic, $M = 0.75$, $J = 3.12$, blade angle 60.2 deg, $r = 1.5$, and $\theta = 90$ deg.

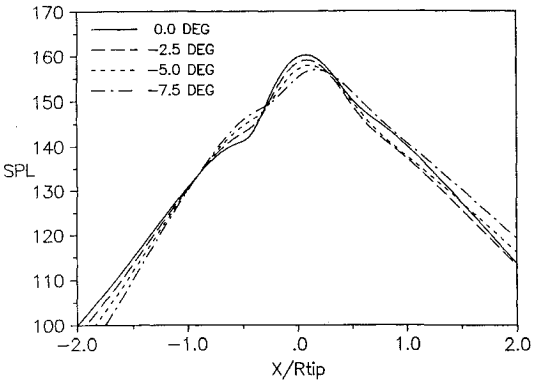

Fig. 15 SR7a propfan in uniform downwash, first harmonic; conditions as in Fig. 14.

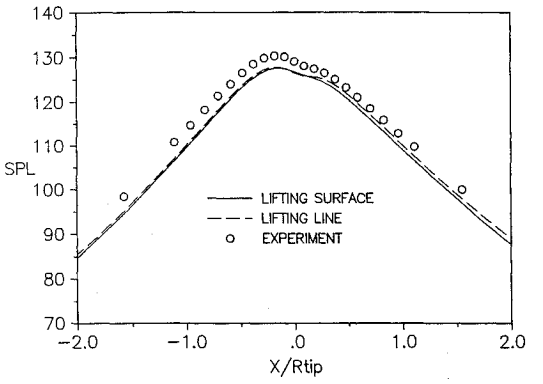

Fig. 16 Fokker 50 propeller, first harmonic, $M = 0.121, J = 0.579$, blade angle 28.0 deg, and $r = 1.323$; lifting line results and experimental data from Ref. 22.

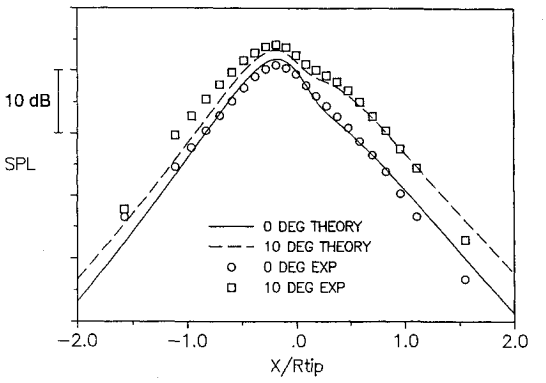

Fig. 17 Fokker 50 propeller, first harmonic SPL at 0 and 10 deg of upwash, $M = 0.23, J = 0.99$, blade angle 36.0 deg, $r = 1.323$, and $\theta = -90$ deg; experimental data from Ref. 14.

the so-called retarded blade shape, or acoustic planform, covers a large part of the propeller disk; for example, see Wells and Han.[21] This phenomenon implies that the sound observed in a field point is composed from signals emitted by the blades during a significant part of their revolution period.

Results for Conventional Propellers

Although the present method was primarily developed for advanced, wide-chord propellers, it can also be applied to conventional propellers. This not only broadens the class of useful experimental data for validation, but also allows a comparison with the results of lifting line methods that are limited to conventional propellers.

As an example of a conventional propeller the 6-bladed Fokker 50 propeller (Dowty Aerospace Propellers, Gloucester, England, United Kingdom) was selected. In Fig. 16 a comparison is made between the first harmonic SPL computed by the present acoustic lifting surface method, a lifting line method,[22] and experimental wind-tunnel data[14] for zero angle of attack of the propeller axis. It is obvious that the agreement between the theories is excellent. Both theories underpredict the experimentally measured acoustic data, although the aerodynamic loading for this heavily loaded case is quite accurately computed. This may be a consequence of the fact that both theories are linear and do not include the nonlinear quadrupole field sources.

In Fig. 17 the measured SPL for 0 and 10 deg of upwash is compared with computed results. Since this propeller rotates in the negative direction a sound increase can be expected at negative azimuthal angles. In general, the agreement is satisfactory, especially in the downward arc. In the forward arc the measured results for 10 deg are somewhat higher than the corresponding computed results. Possibly this is caused by spurious reflections on the measuring equipment, which could not always be avoided in the tests.

Conclusions

A lifting surface method for advanced high-speed propellers has been successfully developed. Aerodynamic and sound calculations based on this method have been carried out for both an advanced high-speed propeller and a conventional propeller in axial and nonaxial flow. In general, the computed results compare well with experimental data.

From sample calculations for the first harmonic it appears that the peak noise level at a representative near-field side line increases with upwash. The typical rate of this increase, however, is not constant but varies from 1.2 dB/deg of upwash at moderate speed to 0.4 dB at high speed.

For downwash the peak level initially falls but starts to rise beyond a certain angle. This limits the peak sound level reduction to a maximum of about 5 dB for the cases investigated.

At supersonic helical tip speeds downwash provides only a marginal possibility to reduce the peak level.

Apart from a peak noise reduction, downwash tends to shift the peak level location in a downstream direction.

Acknowledgment

The present work was supported under Contract 01108N by the Netherlands Agency for Aerospace Programs NIVR.

References

[1]Ffowcs Williams, J. E., and Hawkings, D. L., "Sound Generation by Turbulence and Surfaces in Arbitrary Motion," *Philosophical Transactions of the Royal Society of London*, Series A, Vol. 264, 1969, pp. 321–341.

[2]Gutin, L., "On the Sound Field of a Rotating Propeller," NACA TM 1195, Oct. 1948 (translated from *Physikalische Zeitschrift der Sowjetunion*, Bd. 9, Heft 1, 1936, pp. 57–71).

[3]Garrick, I. E., and Watkins, C. E., "A Theoretical Study of the Effect of Forward Speed on the Free Space Sound Field around Propellers," NACA TN 3018, Oct. 1953.

[4]Farassat, F., "Prediction of Advanced Propeller Noise in the Time Domain," *AIAA Journal*, Vol. 24, No. 4, 1986, pp. 578–584.

[5]Long, L. N., and Watts, G. A., "Arbitrary Motion Aerodynamics Using an Aeroacoustic Approach," *AIAA Journal*, Vol. 25, No. 11, 1987, pp. 1142–1148.

[6]Hanson, D. B., "Direct Frequency Domain Calculation of Open Rotor Noise," *AIAA Journal*, Vol. 30, No. 9, 1992, pp. 2334–2337.

[7]Kondo, K., "On the Potential-Theoretical Fundamentals of the Aerodynamics of Screw Propellers at High Speed," *Journal of the Faculty of Engineering, Univ. of Tokyo*, Vol. 25, No. 2, 1957, pp. 1–39.

[8]Davidson, R. E., "Linearized Potential Theory of Propeller Induction in a Compressible Flow," NACA TN 2983, Sept. 1953.

[9]Hanson, D. B., "Compressible Helicoidal Surface Theory for Propeller Aerodynamics and Noise," *AIAA Journal*, Vol. 21, No. 6, 1983, pp. 881–889.

[10]Schulten, J. B. H. M., "Aerodynamics of Wide-Chord Propellers in Non-Axisymmetric Flow," Paper No. 7, AGARD CP 366, Oct. 1984.

[11]Hanson, D. B., "Noise Radiation of Propeller Loading Sources with Angular Inflow," AIAA Paper 90-3955, Oct. 1990.

[12]Mani, R., "The Radiation of Sound from a Propeller at an Angle of Attack," NASA CR 4264, Jan. 1990.

[13]Nallasamy, M., and Groeneweg, J. F., "Unsteady Blade-Surface Pressures on a Large-Scale Advanced Propeller: Prediction and Data," *Journal of Propulsion and Power*, Vol. 7, No. 6, 1991, pp. 866–872.

[14]Zandbergen, T., Sarin, S. L., and Donnelly, R. P., "Experimental/Theoretical Investigation of the Sound Field of an Isolated Propeller, Including Angle of Incidence Effects," AIAA Paper 90-3952, Oct. 1990.

[15]Woodward, R. P., "Measured Noise of a Scale Model High Speed Propeller at Simulated Takeoff/Approach Conditions," NASA TM 88920; also AIAA Paper 87-0526, Jan. 1987.

[16]Schulten, J. B. H. M., "Sound Generation by Ducted Fans and Propellers as a Lifting Surface Problem," Ph.D. Thesis, Dept. of Applied Mathematics, Univ. of Twente, Enschede, The Netherlands, Feb. 1993.

[17]Crighton, D. G., "Basic Principles of Aerodynamic Noise Generation," *Progress in Aerospace Science*, Vol. 16, No. 1, 1975, pp. 31–96.

[18]Goldstein, M. E., *Aeroacoustics*, McGraw–Hill, 1976, p. 192.

[19]Schulten, J. B. H. M., "Advanced Propeller Performance Calculation by a Lifting Surface Method," AIAA Paper 95-3035, July 1995.

[20]Van de Vooren, A. I., and Zandbergen, P. J., "Noise Field of a Rotating Propeller in Forward Flight," *AIAA Journal*, Vol. 1, No. 7, 1963, pp. 1518–1526.

[21]Wells, V. L., and Han, A., "Geometrical and Numerical Considerations in Computing Advanced-Propeller Noise," *Journal of Aircraft*, Vol. 30, No. 3, 1993, pp. 365–371.

[22]Brouwer, H. H., "On the Use of the Method of Matched Asymptotic Expansions in Propeller Aerodynamics and Acoustics," *Journal of Fluid Mechanics*, Vol. 242, Sept. 1992, pp. 117–143.